IOP Publishing Journal of Optics
J. Opt. **23** (2021) 065001 (10pp) https://doi.org/10.1088/2040-8986/abf8cd

All-optical logic gates based on anomalous Floquet photonic topological insulator structures

Juan M Merlo[1,2,*], Xueyuan Wu[2], Krzysztof Kempa[2] and Michael J Naughton[2]

[1] Physics and Astronomy Department, Vassar College, 124 Raymond Ave, Poughkeepsie, New York 12603, United States of America
[2] Department of Physics, Boston College, 140 Commonwealth Ave., Chestnut Hill, MA 02467, United States of America

E-mail: jmerloramirez@vassar.edu

Received 7 January 2021, revised 1 April 2021
Accepted for publication 16 April 2021
Published 30 April 2021

Abstract

Topological photonics is an incipient research area where the well-developed theory and applications of so-called topological insulators is applied to photonic systems. In that vein, specially-designed ring waveguides, arranged in a periodic structure and evanescently coupled, have shown the ability to propagate edge states that are robust against defects in the lattice. Here, we propose the application of photonic topologically-protected edge states (TPES) in the anomalous Floquet photonic topological insulator structures to develop a device that is able to behave as OR, AND, and XOR logic gates, depending on the characteristics of the excitation field. Materials and dimensions of the device are amenable to conventional fabrication methods, opening the possibility for implementation in on-chip photonic communication technology. We conclude by applying our results to the implementation of an all-optical two bit calculator based on TPES, a potential building block for future computational technology.

Supplementary material for this article is available online

Keywords: photonic topological insulators, nanophotonics, all-optical logic gates

(Some figures may appear in colour only in the online journal)

1. Introduction

Topological photonics constitute a current and expansive research area where the properties of electronic topological insulators (TIs) are evoked with the use of electromagnetic fields in specially-designed materials and structures [1, 2]. Actually, the electronic TIs express their topological properties on electrical currents [3], while photonic topological insulators (PTIs) use electromagnetic waves to perform the topological protection [1, 2, 4, 5]. The notion of a PTI is due to Haldane [6], who proposed the use of non-reciprocal media breaking time-reversal symmetry in a photonic crystal. Many interesting demonstrations have been reported on this matter [5–8], including unidirectional waveguides [9, 10]. Although the vast majority of PTI reports have used photonic crystals [5–10], a different approach is the use of evanescently-coupled ring waveguides [11, 12]. In this configuration, a crystalline-like structure of alternating resonant and non-resonant rings was used and it was possible to emulate the characteristic edge states reported in PTIs. The first demonstration of ring-based PTIs was reported in [11], opening a new avenue for photonic devices applicable to modern on-chip technology.

In the realization of PTIs based on ring waveguides, two approaches have been reported: (a) a configuration that resembles the quantum Hall effect, where a synthetic magnetic field is generated by an additional phase in the circulation of light in a lattice of the PTI, depending on the direction

* Author to whom any correspondence should be addressed.

of circulation [11, 12], and (b) a symmetric configuration that does not depend on a synthetic magnetic field, but ensures the appearance of topologically-protected edge states (TPES) [13–16], emulating the anomalous quantum Hall effect. Due to the absence of broken time-reversal symmetry in the second case, one can find topologically non-trivial phases with robust topologically-protected edge modes, but with Chern number equal to zero [12]. This is enforced by the fact that the Chern number of a band must remain equal to the difference between the numbers of chiral edge modes entering the band from below and exiting above. However, in contrast to static two-band systems (e.g. Haldane model [6]), where each band introduces only one chiral mode into the gap, in Floquet periodically-driven systems, the spectrum is not bound, and thus each band has an equal number of chiral modes below and above, necessarily zeroing the Chern numbers [14].

Here we confirm that, as predicted theoretically [14], our proposed circuitry based on the ring waveguides can be exactly mapped to a driven Floquet system, which can support protected edge states even though the relevant Chern numbers are zero. Specifically, we propose the use of TPES to configure all-optical logic gates working in the visible frequency range, using PTIs based on a symmetric arrangement of ring waveguides. This is the first report of an all-optical logic gates configuration using topologically-protected edge photonic states in the visible. We also show the robustness of the propagation of light in the proposed device by inserting defects in the lattice. Finally, we demonstrate the first all-optical two bits calculator based on TPES. The design can be applied to a wide range of frequencies and a larger number of logic gates to perform complex calculations. We also note that the numerical finite element method (FEM) simulations of Maxwell's equations employed in this work are essentially exact.

2. Methods

For numerical simulations, we used the FEM, COMSOL RF module [17], in two dimensions. We simulated the use of TiO_2 ring waveguides immersed in vacuum. The refractive index of the TiO_2 waveguides was assumed constant and equal to 2.85 (at the working frequency), while the surrounding medium was considered to be 1.00. The difference between refractive indices ensures strong dielectric contrast, allowing for sufficient confinement of photonic modes. Our model was 2D (essentially exact for ring thickness $\gg$ wavelength). The minimum mesh size was 1 nm while the maximum was 20 nm. The frequency used for the demonstrations of logic gates was fixed at 451 THz (665 nm free space wavelength). The excitation field was polarized in the direction pointing out of the page in figure 1(a). The input E-field is delivered at the excitation port (input A/B) while the transmission was measured at the output port, see figure 1(a). Finally, the geometrical characteristics of the waveguides are the same for all results discussed, i.e. mode $m = 20$ and waveguide width 100 nm.

A schematic representation of the device is shown in figure 1(a), where the inset shows the geometrical definition of the separation gap (SG) and the positions of each site ring (SR) and link ring (LR). Here, the SG is an important factor as the evanescent coupling between adjacent rings depends on it, as we will describe below.

3. Results

3.1. All-optical Floquet photonic topological insulator (AFPTI) design

With an aim of emulating the special properties of TIs, the search for equivalent interactions using light has resulted in a simple approximation. As analogs of atomic centers, where electrons are bound and resonating at different energies, photonic resonant cavities have been used [12]. In the case we present here, rings can accomplish this with the resonant condition $\beta\, L_{SR} = 2\,\mathrm{m}\pi$, with β the effective wavenumber of the propagated mode, L_{SR} the length (circumference) of the ring, and integer m the mode order. We call these the SRs. On the other hand, in the place of evanescent coupling among atomic sites, so-called LRs are used. LRs are antiresonant by design ($\beta\, L_{LR} = \beta\, L_{SR} + \pi$, with L_{LR} the length of the LR), meaning light was not allowed to generate a standing wave and consequently coupling to the next SR. With these definitions, one can see that our design, in principle, emulates a crystalline structure where light takes the place of electrons in a condensed matter system. As our interest is in the application of AFPTIs, we do not present a theoretical analysis of the physics of resonant waveguides, nor the well-known theory of TIs, which can be found elsewhere [18, 19].

3.2. Interaction coupling

In an AFPTI system, here composed of a symmetric arrangement of ring waveguides, it is customary to make use of transmission and coupling factors, t and k, respectively, to describe the interaction strength among the rings [16]. However, a different approach reported in the literature is a parameterization that results in a coupling strength factor (CSF) defined by $\theta = \sin^{-1}(I_{out}/I_{in})$, where I_{in} and I_{out} are the input and output optical intensities, respectively [13, 14]. In fact, three characteristics of AFPTI devices based on ring waveguides are well-accepted: (a) weak-interactions are characterized by $\theta < \pi/4$; (b) the topological transition occurs when $\theta \sim \pi/4$; and (c) strong-interactions, where robust edge modes appear, when $\theta > \pi/4$, for smaller distances than the topological transition [13]. We analyzed the CSF for a set of SGs and frequencies as shown in figure 1(b), where the color scale ranges only to values that showed topological effects ($\theta > \pi/4$). For the particular case when the frequency is 451 THz, we found the topological transition ($\theta \sim \pi/4$) at SG $\sim$ 50 nm, and the strong interaction ($\theta > \pi/4$) at SG $\sim$ 40 nm, see the shaded zone in figure 1(c). In this particular case, assuming lossless waveguides, the coupling strength, defined as $k^2 = 1 - I_{out}/I_{in}$ [18], resulted $k = 0.38$.

In order to confirm the topological behavior of the proposed device, where a strong interaction region was found, see figure 1(c), we calculated the band diagram for a set of SGs where this condition was matched. The results are shown

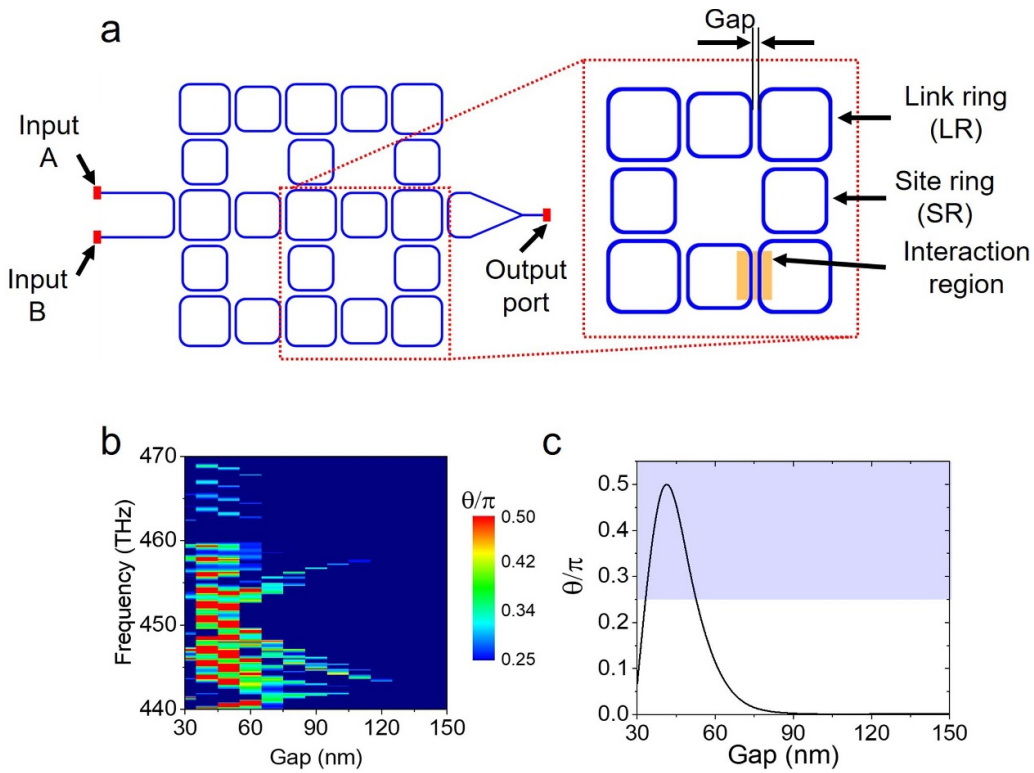

Figure 1. Description of the proposed device. (a) Schematic representation of a photonic topological insulator based on rectangular rings and consisting of 2 × 2 lattices. The blue lines represent dielectric (e.g. TiO_2) waveguides and the red points the input and output ports. Inset: detail of a lattice area defining the separation gap (SG) as well as the position of site ring (SR) and link ring (LR). The shaded region represents the interaction area between two rings. (b) Coupling strength factor (θ) as function a of separation gap and operation frequency. (c) Coupling strength factor at 451 THz, for separation gaps running from 30 nm to 150 nm. The shaded region highlights the gap sizes for strong coupling.

in figure 2, where it can be seen that the topological transition occurs for SG $\sim$ 50 nm, while the robust edge modes emerge near SG $\sim$ 40 nm. A clear signature of topological behavior was the collapse of the bulk band to a point (SG $\sim$ 50 nm) [13, 14], and to reopen later (e.g. for SG $\sim$ 40 nm), allowing the edge modes to appear, blue and orange lines in figure 2 for SG = 40 nm. Details on the band diagram calculations and the transmission of the device can be found in the supplementary information (SI) (available online at stacks.iop.org/JOPT/23/065001/mmedia).

In figure 3, we report the mode profiles selected at the triangle and star marks in figure 2 for SG = 40 nm. In the case of the bulk mode, figure 3(a) (triangle for SG = 40 nm in figure 2), light was transmitted through the body of the device, while for the edge mode, it followed the perimeter of the device (star for SG = 40 nm in figure 2), i.e. as an edge mode. Additionally, figure 3(c) demonstrates the robustness of the TPESs; after removing one lattice site, the mode continued propagating along the new, modified edge. These images confirm the topological behavior of our device and allow us to be confident of the analysis presented in this work. In the SI, we show a 3 × 3 device where a set of defects was included in order to make clear the robustness of the TPES against disorder in a larger lattice. Also, in the SI, it can be found the case in which a SR is broken. In such a situation, the electromagnetic field propagation is strongly disrupted, however, the energy propagating in the device could find a new edge to propagate. Finally, the perturbation of the structure of the PTI can be done by altering the shape of one of the SRs. In such a case, the energy propagation found a new edge closer to the original one, see SI.

With respect to the selected shape of the rings, i.e. rectangular with rounded corners as seen in figure 1(a), it is well known that the interaction between circular rings is confined to a small region that tends to a single point [13]. In such a case, the requirements to reach the strong coupling regime—where evanescent coupling is sufficient to excite modes between neighboring rings—are very tight, meaning the topological transition occurs when SG $\sim$ 25 nm and robust edge modes appear for SG $\sim$ 10 nm (see SI). Such geometrical characteristics generate a very challenging device for current fabrication technologies if an experimental demonstration is to be pursued. On the other hand, the geometry presented in this work increases the interaction region, relaxing the SG requirements. We found that as the interaction region increases in length, see figure 1(a), the topological transition runs to greater SGs, a convenient effect for a fabrication procedure, though radiation losses due to defects in a real device can still affect the final output. In this sense, we have chosen an interaction region length of 4 μm, meaning $m = 20$ in the resonance condition, in which case the topological transition happens at SG $\sim$ 50 nm, and the robust edge modes occur at SG $\sim$ 40 nm, as discussed

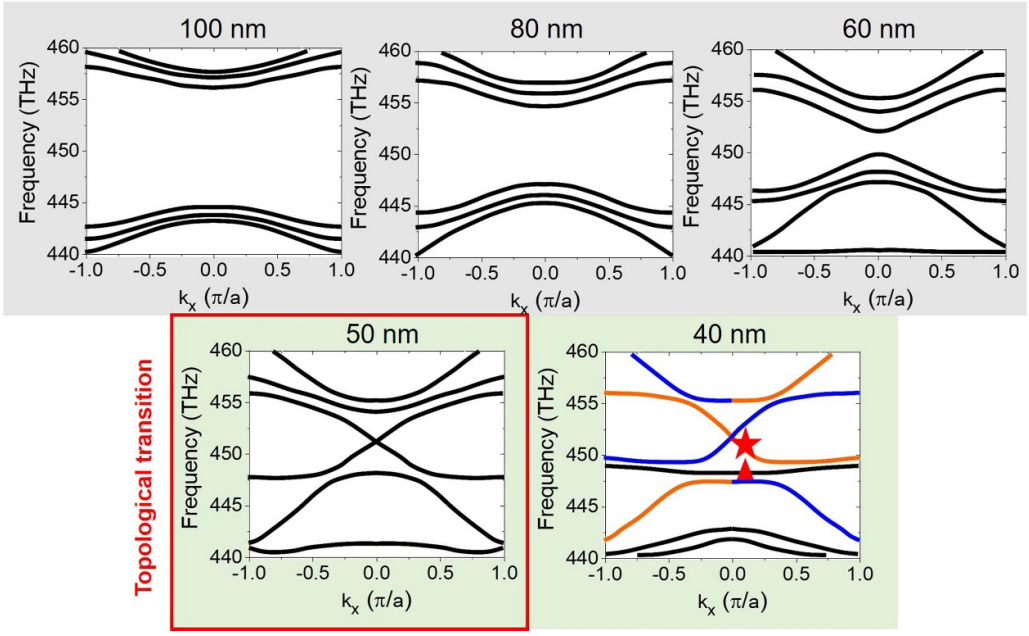

Figure 2. Band diagram as a function of the separation gap. The numbers in the top of each image represents the separation gap (SG). The red frame remarks the topological transition for SG = 50 nm. The blue and orange lines for SG = 40 nm represent edge modes, as described in the main text. The gray and green shades represent the weak- and strong-interaction regions, respectively.

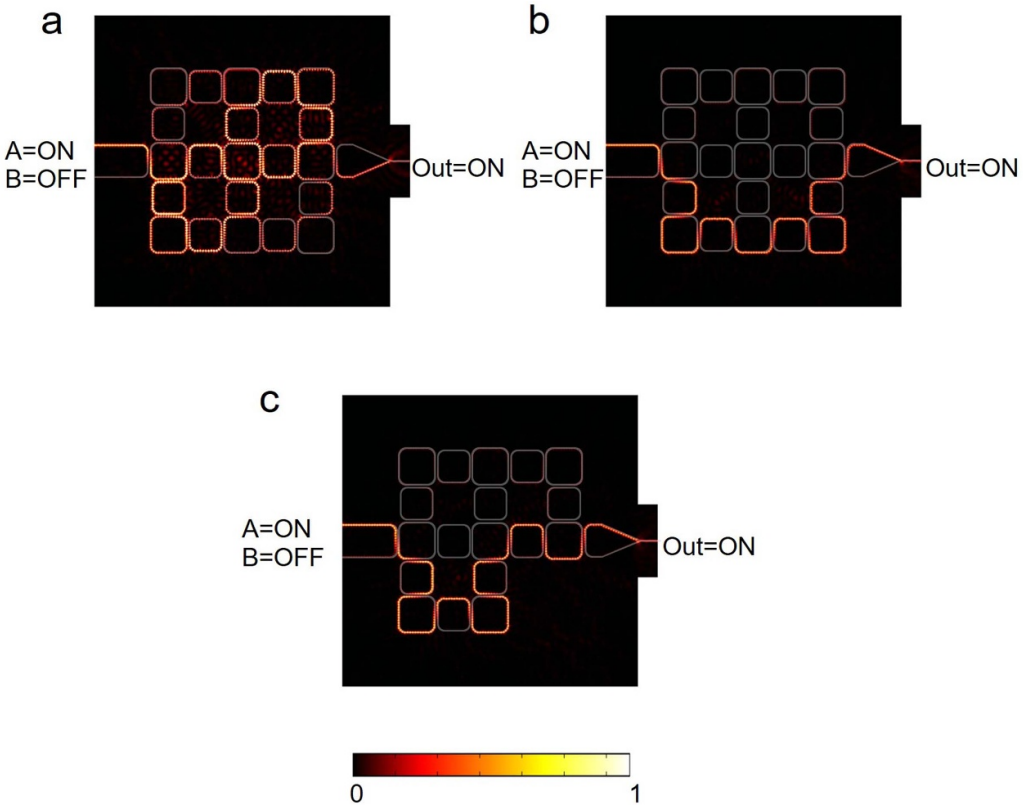

Figure 3. Normalized intensity distribution in the TPES device. (a) Bulk mode for 448 THz. (b) Edge mode for 451 THz. Both (a) and (b) were selected from frequencies highlighted as triangle and star, respectively, in figure 2 for SG of 40 nm. (c) Robustness of the edge mode when a lattice site is removed. In all the images, the shapes represent the waveguides in the device.

above. It is possible to fabricate these devices by using electron beam lithography with positive resist, and a deposition of TiO_2 by electron beam evaporation should ensure the correct deposition of the structures.

Additionally, we note that our systematic study has two different characteristics with respect to other reports where resonant rings were used: (a) in [10–12], the circulation phase along a single lattice was used as a pseudo-energy in the band

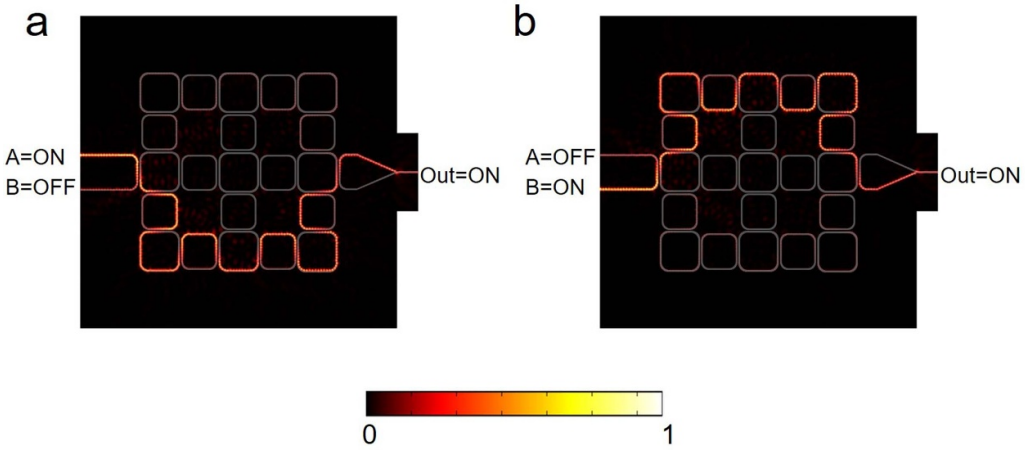

Figure 4. Demonstration of the symmetric propagation of TPES. (a) Input A = ON results in an output of ON. (b) Input B = ON results in an output of ON.

diagrams. Contrarily, we report frequency band diagrams, i.e. real energy diagrams, offset by a factor equivalent to Planck's constant; (b) previously, the CSF was varied freely as a theoretical value without any sense of the characteristics of the crystal lattice [11, 13]. Our work, on the other hand, reports CSF as a function of SG, offering better insight into the geometrical properties of the device, and providing a clearer idea of possible fabrication limitations.

3.3. *All-optical logic gates*

After confirming the topological behavior of the proposed device, we now turn our attention to the application of its special properties. We focus on a particular application, an all-optical logic gate. Some previous configurations of all-optical logic gates have been reported to the date [20, 21]. However, none of them used the special properties of a TPES as proposed in this work.

In order to simplify the discussion of the current results, we use ON/OFF states accordingly to the binary code, i.e. ON = 1 and OFF = 0. For the case of the output, we consider a state to be ON (OFF) when there is energy crossing (not crossing) the output port, see figure 1(a)).

In addition, a TPES in the proposed device has two possible paths to propagate, meaning there is a protected state at the upper edge of the device (A = ON, B = OFF) as well as in the lower edge (A = OFF, B = ON), as shown in figure 4. Thus, the symmetry of the device has as an important consequence, i.e. the ability to control the output by using one of two methods, described as follows:

3.3.1. Mode 1. ON/OFF of the excitation energy at the A/B inputs. For this mode, we took advantage of the fact that the device will propagate light only when excitation energy is applied to one or both of the inputs, meaning output ON for A/B in ON state, and output OFF for A/B in OFF state.

3.3.2. Mode 2. Phase difference between A/B inputs. Here, we used the symmetric behavior of the device, see figure 4. It is clear that the output can be controlled by interference of the incoming light in the triangular ring at the output port. As such, when the phase difference between inputs A and B was 0, the output is ON, and OFF for a phase difference of π.

Using these controls, it is possible to develop a set of all-optical logic gates, particularly OR, AND, and XOR logic, among the most important components of modern electronic technology [22]. We chose these logic gates because it is possible to perform basic calculations using them, as we will show later.

3.3.3. OR gate. In the case of the OR gate, the excitation energy was turned ON/OFF as commented in Mode 1 above. In this way, when A and B were ON, or when A or B are ON, the output was ON; when both A and B are OFF, the output was OFF. This behavior was, as expected, the OR logic [22]. In figure 5, we show the results of the OR logic gate based on TPES. There, the intensity of the optical field is normalized and in the cases of figures 5(b) and (c), the intensity was enhanced by 50% for easier observation of the behavior of the electromagnetic field in the device. It is important to note that even when the output intensity was smaller as in the latter cases, the switching action was still sufficient to distinguish between the ON and OFF states at the output. When both inputs were in OFF state, the output was OFF, a trivial case that we do not show in figure 5.

3.3.4. XOR gate. The difference between OR and XOR logic is that, in the case of an XOR gate, the output is OFF when both inputs A and B are ON [22]. By using phase control (Mode 2), with a phase difference of $\phi = \pi$ between inputs A and B, the result was an output OFF even when A and B were ON, see figure 6(a). For the next cases, the logic was not different from the OR logic, that is, when A or B were ON, the output was ON, figures 6(b) and (c), respectively, and when the inputs were both OFF, the output was OFF. This last case is not shown in figure 6, as it is also the trivial case. The control of the phases in this situation could be done by using

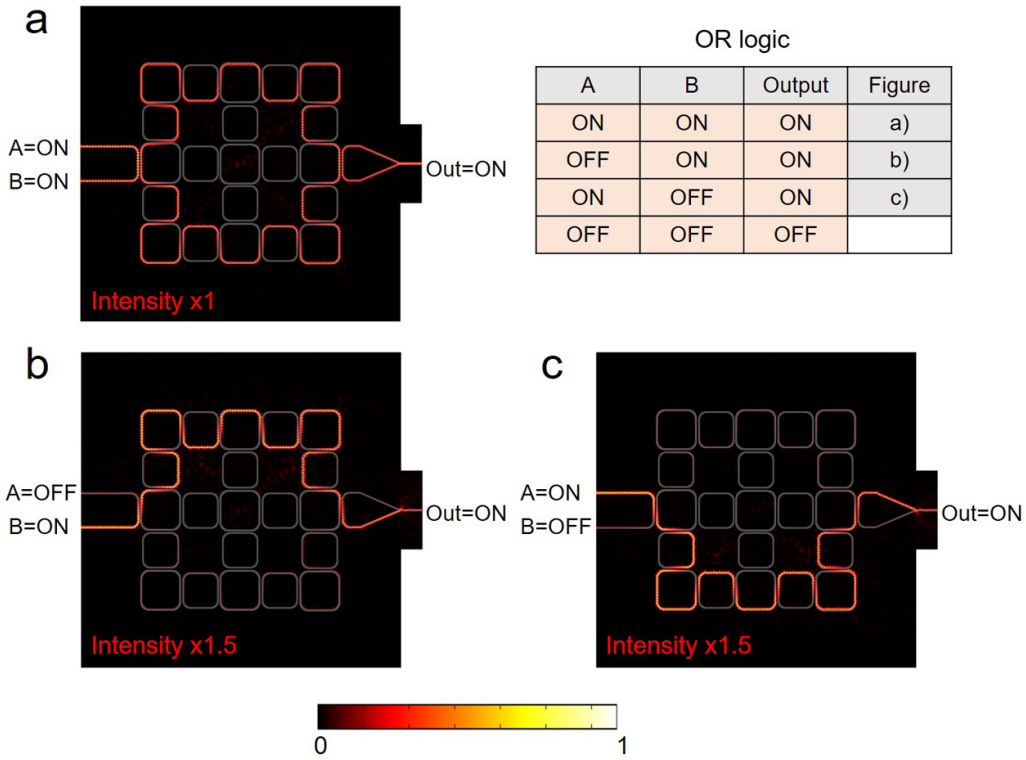

OR logic

A	B	Output	Figure
ON	ON	ON	a)
OFF	ON	ON	b)
ON	OFF	ON	c)
OFF	OFF	OFF	

Figure 5. Demonstration of the OR logic in the proposed device. (a) Inputs A and B are ON, resulting in an output of ON. (b) Input B is ON and A is OFF, resulting in an output of ON. (c) Input A is ON and B is OFF, resulting in an output of ON. The inset shows the OR logic table (Mode 1).

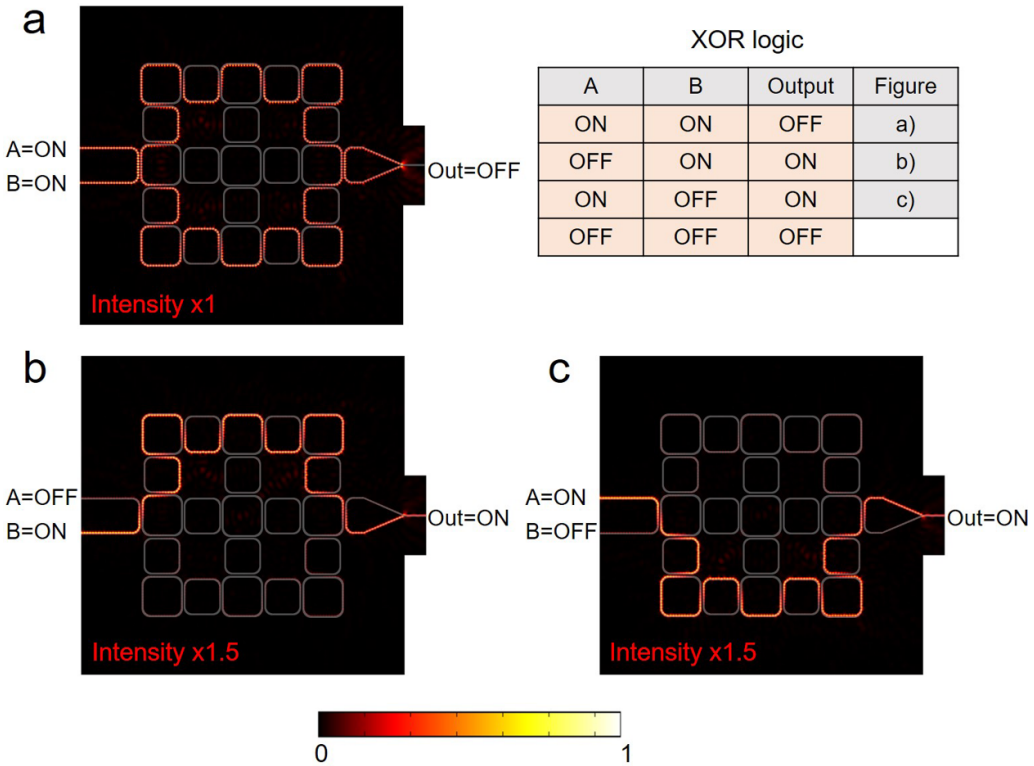

XOR logic

A	B	Output	Figure
ON	ON	OFF	a)
OFF	ON	ON	b)
ON	OFF	ON	c)
OFF	OFF	OFF	

Figure 6. Demonstration of the XOR logic in the proposed device. (a) Inputs A and B are ON with phase difference of $\phi = \pi$, resulting in an output OFF. (b) Input B is ON and A is OFF, resulting in an output of ON. (c) Input A is ON and B is OFF, resulting in an output of ON.

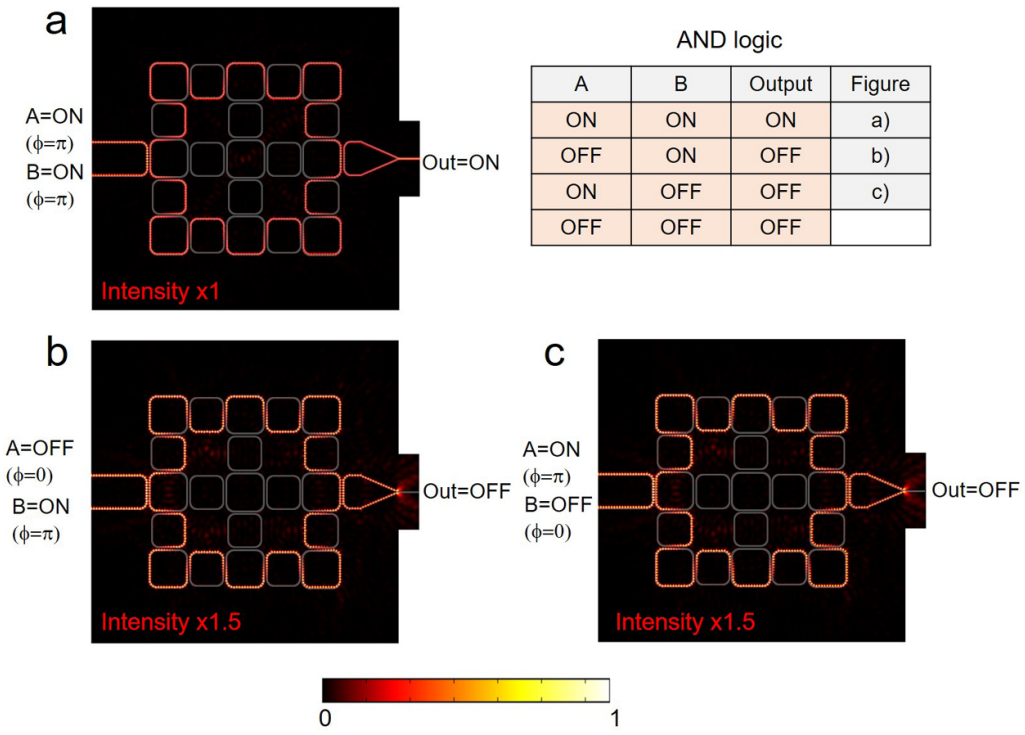

Figure 7. Demonstration of the AND logic in the proposed device. (a) The inputs A and B are ON with phase difference $\phi = 0$, resulting in an output ON. (b) The input B is ON and A is OFF resulting in an output of ON. (c) The input A is ON and B is OFF resulting in an output of ON. The inset shows the AND logic table.

a refractive index shift using electronic means as that shown in [23].

3.3.5. AND gate. In this case, we controlled the device by shifting the phase between the A and B inputs (Mode 2). We define the ON signal when the excitation input had a phase of $\phi = \pi$, and OFF when it had phase of $\phi = 0$. In this way, when A and B were ON, the output was ON, and when A was ON/OFF and B was OFF/ON, the output was OFF, see figure 7. Although we have defined the ON/OFF states in terms of the phase difference between the inputs to obtain AND logic, we could also get the OFF state at the output by turning off the excitation energy in both inputs to complete the logic, see table in figure 7.

3.4. Two bit calculator based on TPES logic gates

In order to demonstrate the ability of the proposed device to be used as building block of an all-optical computer, we have performed a basic computation in a simple calculator made by the combination of XOR and AND logic gates, also called a half-adder [22]. This calculator had two inputs (A, B) and two outputs, called the lowest significant bit (LSB) and the most significant bit (MSB), and we consider this application a two bit calculator. Using this rudimentary computation device, we calculated the sums $1 + 0$ and $1 + 1$, i.e. ON plus OFF and ON plus ON in our schemes, with expected decimal results of $1 + 0 = 1$ and $1 + 1 = 2$, but in binary code LSB $= 1$ (1) and MSB $= 1$ (2). The summarized results are presented in figure 8.

The most important advantage of using the topological nature of the proposed logic gates, is that the inclusion of defects in the structure of the components of the proposed calculator had null effect on the results, ensuring an outstanding performance compared with any non-topological device [20, 21].

3.5. Robustness of the calculator

As stated above, one of the most important features of the proposed device is its robustness, i.e. calculations are not affected by inclusion of defects. Using the same device as before, figure 8, we performed the calculation of decimal $1 + 1 = 2$ or in binary code LSB $= 0$ and MSB $= 1$, just to show an example. It is clear that the result was not affected by the inclusion of strong defects in one of the components, see figures 9(b)) and (c)). More important was that with the inclusion of defects representing more than one lattice site in each device, the calculation was still performed correctly, see figures 9(d)) and (e)). We note that this robustness demonstration was only achievable by the use of TPESs that continue to propagate although the shape of the device has changed.

3.5.1. Conventional waveguides (CWs) vs topological devices. It is natural to ask for the use of TPESs in devices that have been proven so far with CWs, and the answer lies in the fact that the CWs are not able to propagate light around

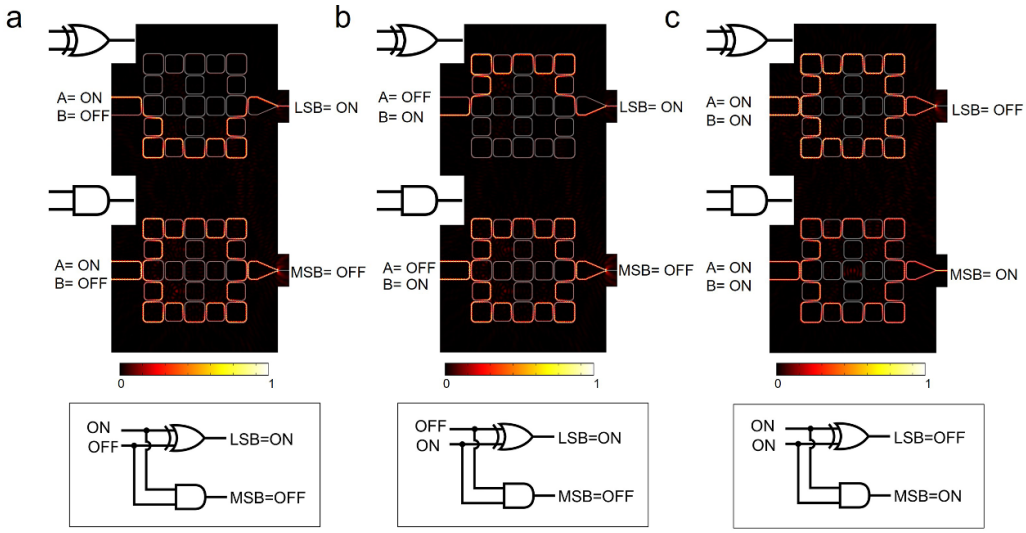

A	B	Operation	Result	Binary output		Figure
				MSB	LSB	
ON	OFF	1+0	1	0	1	a)
OFF	ON	0+1	1	0	1	b)
ON	ON	1+1	2	1	0	c)

Figure 8. Demonstration of the two bit computer. (a) Sum of $1 + 0$ (A = ON and B = OFF) resulting in LSB = 1 (ON) or decimal 1. (b) Sum of $0 + 1$ (A = OFF and B = ON) resulting in LSB = 1 (ON) or decimal 1. (c) Sum $1 + 1$ (A = ON and B = ON) resulting in MSB = 1 (ON) or decimal 2. The inset shows a table with the equivalent operations demonstrated in this section.

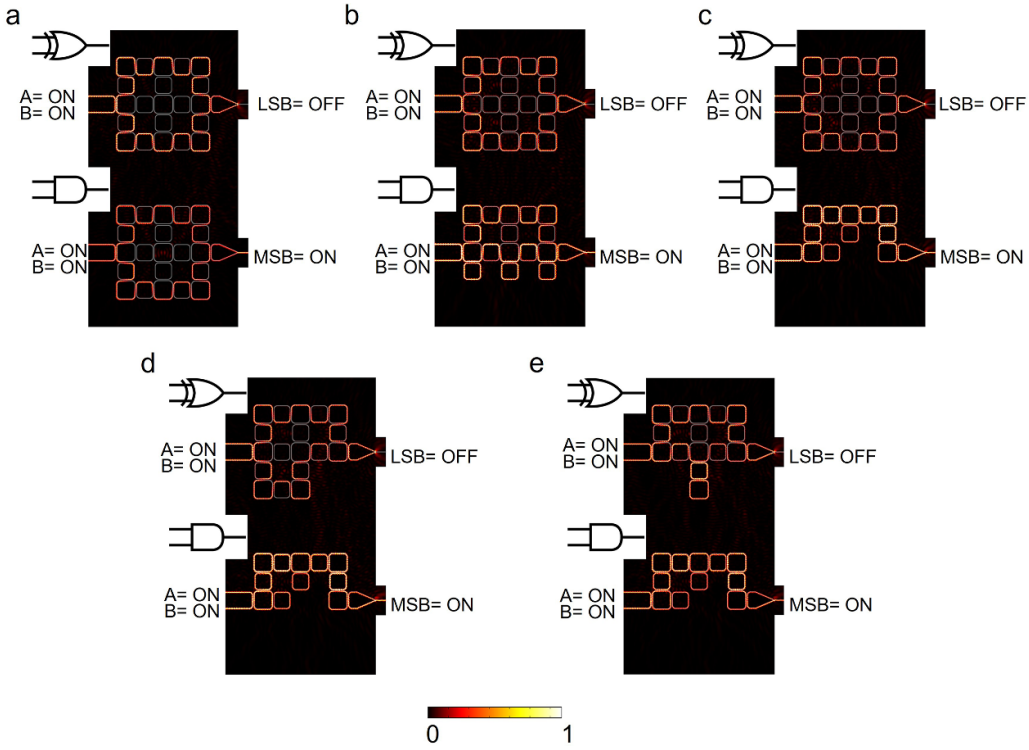

Figure 9. Demonstration of the robustness of the calculation of $1 + 1$. (a) XOR and AND gates with no defects on their structure. (b) Three SR and LR defects on AND gate, no defect on XOR. (c) Four SR and LR defects on AND gate, no defect on XOR. (d) Four SR and LR defects on AND gate and one lattice site defect on XOR. (e) Four SR and LR defects on AND gate and four SR and three LR defects on XOR.

sharp turns, defined here as 90° turns, without the use of a large radius of curvature. Moreover, CWs cannot keep the transmitted signal in an efficient way when defects on the waveguide are included. We report an analysis of such cases in the SI. There, one can see how the TPES could overcome both the loss of energy in sharp turns and the addition of defects. Indeed, the inclusion of up to four sharp turns in CWs reduced the transmitted power more strongly than that reported by the topological devices, see figure S6.

3.5.2. Phase control. Finally, another important concern was the control of input phase as used in the Mode 2. Figure S8 in the SI shows the performance of the device output as a function of the phase difference between the inputs. It is clear that the switching action due to phase difference was very robust and would remain useful even when it was affected by ∼30% for a phase difference of $\sim\pm\pi/2$.

4. Discussion and summary

One of the building blocks of future all-optical computers will be all-optical logic gates [21, 24]. However, few advances have been done in this direction. The proposed device in the present work opens the possibility to integrate logic gates by composing different arrangements of all-optical devices based on TPES with a single device. Moreover, the ability of this device to use visible light—easily extended, but not limited, to the near IR for silicon photonics—for facile control of the output signal, and the robustness against disorder, makes this a potentially valuable technology to be applied in the pursuit of all-optical computation. Also, as can be seen in figure 2, there is a broad spectrum where the TPES can be found, this means that the proposed device can perform different logic operations at different frequencies, enhancing its potential applications. It is important to remark that, although in this work we showed the application of a calculator with two bit capacity and the demonstration of the sum of 1/0 + 0/1 and 1 + 1, the concept can be expanded to any number of bits to perform complex calculations.

In summary, all-optical logic gates using TPES were demonstrated by numerical models. By a systematic numerical analysis, we determined optimal geometric configurations when TiO_2 rectangular ring waveguides were used at 451 THz. These geometrical characteristics allow fabrication of devices using modern technologies having high-resolution lithography. Using two simple methods for output signal control, we showed how a single device can operate as an OR, XOR, or AND gate. We also showed that, due to the topological nature of the device, inclusion of strong defects in the device structure do not affect the overall output. Finally, we consider the most important contribution of the present work to be the fact that the results obtained by the implemented two bit calculator is not affected by the inclusion of defects in the structure of the composing logic gates. The photonic nature of the proposed device allows it to work in the high-speed information transmission range (GHz), limited only by the control of phase commutation, and more importantly, reduced power consumption to levels that electronic devices are not capable of achieving.

Data availability statement

The data that support the findings of this study are available upon reasonable request from the authors.

Acknowledgment

Juan M Merlo acknowledges Vassar College for startup funding number ST000057.

Conflict of interest

The authors declare no conflicts of interest.

ORCID iD

Juan M Merlo https://orcid.org/0000-0002-3956-0940

References

[1] Lu L, Joannopoulos J D and Soljačić M 2014 Topological photonics *Nat. Photon.* **8** 821–9
[2] Wu L H and Hu X 2015 Scheme for achieving a topological photonic crystal by using dielectric material *Phys. Rev. Lett.* **114** 223901
[3] Zhang H, Liu C X, Qi X L, Dai X, Fang Z and Zhang S H 2009 Topological insulators in Bi_2Se_3, Bi_2Te_3 and Sb_2Te_3 with a single dirac cone on the surface *Nat. Phys.* **5** 438–42
[4] He C, Sun X C, Liu X P, Lu M H, Chen Y, Feng L and Chen Y F 2016 Photonic topological insulator with broken time-reversal symmetry *Proc. Natl Acad. Sci.* **113** 4924–8
[5] Xie B Y, Wang H F, Zhu X Y, Lu M H, Wang Z D and Chen Y F 2018 Photonics meets topology *Opt. Express* **26** 24531
[6] Haldane F D M and Raghu S 2008 Possible realization of directional optical waveguides in photonic crystals with broken time-reversal symmetry *Phys. Rev. Lett.* **100** 013904
[7] Wu X, Ye F, Merlo J M, Naughton M J and Kempa K 2018 Topologically protected photonic edge states in the visible in plasmo-gyroelectric metamaterials *Adv. Opt. Mater.* **6** 1800119
[8] Zhirihin D, Filonov D, Gorlach M, Slobozhanyuk A, Kivshar Y and Khanikaev A 2018 Experimental realization of three-dimensional all-dielectric photonic topological insulators *2018 USNC-URSI Radio Science Meeting* (*Boston, MA, 8–13 July 2018*) pp 3–4
[9] Wang Z, Chong Y, Joannopoulos J D and Soljačić M 2009 Observation of unidirectional backscattering-immune topological electromagnetic states *Nature* **461** 772–5
[10] Skirlo S A, Lu L and Soljačić M 2014 Multimode one-way waveguides of large Chern numbers *Phys. Rev. Lett.* **113** 113904
[11] Hafezi M, Demler E A, Lukin M D and Taylor J M 2011 Robust optical delay lines with topological protection *Nat. Phys.* **7** 907–12
[12] Mittal S, Ganeshan S, Fan J, Vaezi A and Hafezi M 2016 Measurement of topological invariants in a 2D photonic system *Nat. Photon.* **10** 180–3

[13] Liang G Q and Chong Y D 2013 Optical resonator analog of a two-dimensional topological insulator *Phys. Rev. Lett.* **110** 203904
[14] Pasek M and Chong Y D 2014 Network models of photonic Floquet topological insulators *Phys. Rev.* B **89** 075113
[15] Gao F *et al* 2016 Probing topological protection using a designer surface plasmon structure *Nat. Commun.* **7** 11619
[16] Rudner M S, Lindner N H, Berg E and Levin M 2013 Anomalous edge states and the bulk-edge correspondence for periodically driven two-dimensional systems *Phys. Rev.* X **3** 031005
[17] COMSOL Multiphysics v5.3a (Stockholm: COMSOL AB) (available at: www.comsol.com)
[18] Poon J, Scheuer J, Mookherjea S, Paloczi G T, Huang Y and Yariv A 2014 Matrix analysis of mirroring coupled-resonator optical waveguides *Opt. Express* **12** 90
[19] Qi X L and Zhang S C 2010 The quantum spin Hall effect and topological insulators *Phys. Today* **63** 33–8
[20] Singh P, Tripathi D K, Jaiswal S and Dixit H K 2014 All-optical logic gates: designs, classification, and comparison *Adv. Opt. Technol.* **2014** 1–13
[21] Jandieri V, Khomeriki R and Erni D 2018 Realization of true all-optical AND logic gate based on nonlinear coupled air-hole type photonic crystal waveguides *Opt. Express* **26** 19845
[22] Shiva S G 1988 *Introduction to Logic Design* First (Illinois: Scott, Foresman and Company)
[23] Lu Z, Celo D, Mehrvar H, Bernier E and Chrostowski L 2017 High-performance silicon photonic tri-state switch based on balanced nested Mach-Zehnder interferometer *Sci. Rep.* **7** 12244
[24] He L, Zhang W X and Zhang X D 2019 Topological all-optical logic gates based on two-dimensional photonic crystals *Opt. Express* **27** 25841–59